

generated January 10, 2014

E(B-V), N(H I) and N(H₂)

Harvey Liszt

*National Radio Astronomy Observatory
520 Edgemont Road, Charlottesville, VA 22903-2475*

hliszt@nrao.edu

ABSTRACT

We consider the structure of the N(H I) - E(B-V) relationship when H I is measured in the 21 cm radio line and E(B-V) is defined by far-IR dust-derived measures. We derive reddening-dependent corrections to N(H I) based on interferometric absorption measurements over the past 30 years that follow a single power-law relationship $\int \tau(HI) dv = 14.07 \text{ km s}^{-1} E(B-V)^{1.074}$ at $0.02 \lesssim E(B-V) \lesssim 3 \text{ mag}$. Corrections to 21cm line-derived H I column densities are too small to have had any effect on the ratio $N(H I)/E(B-V) = 8.3 \times 10^{21} \text{ cm}^{-2} \text{ mag}^{-1}$ we derived at $0.015 \lesssim E(B-V) \lesssim 0.075 \text{ mag}$ and $|b| \geq 20^\circ$; they are also too small to explain the break in the slope of the N(H I) - E(B-V) relation at $E(B-V) \gtrsim 0.1 \text{ mag}$ that we demonstrated around the Galaxy at $|b| \geq 20^\circ$. The latter must therefore be attributed to the onset of H₂-formation and we show that models of H₂ formation in a low density diffuse molecular gas can readily explain the inflected N(H I)- E(B-V) relationship. Below $|b| = 20^\circ$ N(H I)/E(B-V) measured at $0.015 \lesssim E(B-V) \lesssim 0.075 \text{ mag}$ increases steadily down to $|b| = 8^\circ$ where sightlines with small E(B-V) no longer occur. By contrast, the ratio N(H I)/E(B-V) measured over all E(B-V) declines to $N(H I)/E(B-V) = 5 - 6 \times 10^{21} \text{ cm}^{-2} \text{ mag}^{-1}$ at $|b| \lesssim 30^\circ$, perhaps providing an explanation of the difference between our results and the gas/reddening ratios measured previously using stellar spectra.

Subject headings: astrochemistry . ISM: dust . ISM: H I . ISM: clouds. Galaxy

1. Introduction

In an earlier paper (Liszt 2014) we considered the relationship between H I column density N(H I) derived from the large-scale 21cm H I sky surveys (Kalberla et al. 2005; Peek et al. 2011),

and reddening $E(B-V)$ as derived from far IR dust emission by Schlegel et al. (1998) (SFD98). We traced $N(\text{H I})$ and $E(B-V)$ around the sky at galactic latitudes $|b| = 20^\circ - 60^\circ$ and considered data at lower column densities $0.015 \lesssim E(B-V) \lesssim 0.075$ mag, where the hydrogen should be in the form of neutral atoms and corrections to $N(\text{H I})$ for saturation and H_2 -formation are unimportant. We showed that the relevant value of the gas/reddening ratio is $N(\text{H I})/E(B-V) = 8.3 \times 10^{21} \text{ cm}^{-2} \text{ mag}^{-1}$, considerably larger than the usually-cited ratio $N(\text{H})/E(B-V) = 5.8 \times 10^{21} \text{ cm}^{-2} \text{ mag}^{-1}$ derived from optical/uv absorption measurements toward stars by Bohlin et al. (1978), where $N(\text{H}) = N(\text{H I}) + 2N(\text{H}_2)$. It is also larger than the values $N(\text{H I})/E(B-V) = 4.8 - 5.2 \times 10^{21} \text{ cm}^{-2} \text{ mag}^{-1}$ that are consistently quoted for stellar reddening and $\text{Ly-}\alpha$ absorption toward early-type stars (Bohlin et al. 1978; Shull & van Steenberg 1985; Diplas & Savage 1994).

In fact there are two mysteries in the disparity between radio/IR and optical/uv derivations of $N(\text{H})/E(B-V)$. The first is the numerical discrepancy, which puts several 21 cm surveys and the work of SFD98 together on one side in opposition to $\text{Ly-}\alpha$ measurements by several groups using IUE and Copernicus and stellar reddening on the other. The second is the very nearly constant value for $N(\text{H I})/E(B-V)$ quoted for the stellar data, as opposed to the radio-IR relationship shown in Figure 1 of Liszt (2014) that had a very strong point of inflection to smaller $N(\text{H I})/E(B-V)$ at $E(B-V) \gtrsim 0.08$ mag. In principle the inflection in the radio data could reflect either the influence of saturation of the 21cm line profiles or the expected onset of H_2 formation as originally discovered in the uv absorption data (Savage et al. 1977). We noted a seemingly similar inflection in the IUE results of Diplas & Savage (1994), whereby much higher values of $N(\text{H I})/E(B-V)$ were seen at $E(B-V) < 0.1$ mag (their Fig. 4a), but this was not taken into account in their final result. It should also have been present in the earlier treatment of the IUE results by Shull & van Steenberg (1985), who derived very nearly the same numerical result as in the later work.

This work is largely concerned with understanding the change in slope of the radio-IR defined $N(\text{H I})$ - $E(B-V)$ relationship, unravelling the possibly competing effects of 21cm H I line saturation and H_2 -formation. In Section 2 we discuss independent measures of 21cm H I optical depth as a function of reddening, which can be employed to show that saturation corrections to 21cm measurements of $N(\text{H I})$ are small at least until $E(B-V) > 0.3$ mag. In that case, only H_2 -formation can explain the observed inflection. In Sect. 3 we show that rather conventional models of H_2 formation in a low density diffuse molecular gas can reproduce the observed $N(\text{H I})$ - $E(B-V)$ relationship. In Section 4 we extend our analysis to lower galactic latitude $|b| = 9^\circ - 20^\circ$ and show that there are progressively higher values of $N(\text{H I})/E(B-V)$ at all $E(B-V)$ as $|b|$ declines. Section 5 is a brief summary and discussion.

2. Optical depth and saturation correction in the 21cm line

Figure 1 shows an updated and annotated version of the N(H I)-E(B-V) relationship first shown in (Liszt 2014), again using H I profiles from the LAB (Leiden-Argentina-Bonn) all-sky H I survey (Kalberla et al. 2005) and E(B-V) from the work of SFD98. Explaining the annotations and the rather modest saturation correction to N(H I) that has been applied to the data is the subject of the current work. In passing, please note that Figure 1 of Liszt (2014) inadvertently displayed the data for only that half the sky at $0^\circ \leq l \leq 180^\circ$, without affecting the numerical results. Note also that the phenomenon of gas without dust, which manifests itself as high ratios of N(H I)/E(B-V) at small E(B-V), is not clearly present down to reddenings as small as 0.01 mag. Also missing at small values of E(B-V) is a downturn in N(H I) that could have signalled the presence of in increasing fraction of warm ionized gas.

2.1. Systematic variation of the 21cm optical depth with reddening

To understand the possible effects of saturation we began by binning the data in reddening (averaging over all the data comprising Fig. 1) and forming mean H I emission profiles as a function of reddening. Figure 2 shows some of these for $0.025 \text{ mag} \leq E(B-V) \leq 0.33 \text{ mag}$ and it is clear that imputing high optical depth to the profiles around $E(B-V) = 0.1 \text{ mag}$ would require spin temperatures below 30 K for which there is no support in such diffuse gas.

The argument for modest optical depths may be made quantitative by considering the variation of measured 21cm optical depth $\Xi_{\text{HI}} = \int \tau(\text{HI}) dv$ (units of km s^{-1}) with reddening first discussed by Liszt et al. (2010) using a combination of their own more recent VLA data and that measured earlier by Dickey et al. (1983). Liszt et al. (2010) showed that there is a strong, nearly-linear relationship between Ξ_{HI} and E(B-V) but with scant data at higher galactic latitude and with much scatter and sparse data-coverage at $E(B-V) < 0.3 \text{ mag}$. This situation is alleviated by inclusion of the new results of Roy et al. (2013) as shown in Fig. 3¹.

The error-weighted regression line in Fig. 3 is $\log \Xi_{\text{HI}} = 1.147 \pm 0.019 + (1.074 \pm 0.034) \log E(B-V)$ or $\Xi_{\text{HI}} = 14.07 E(B-V)^{1.074}$, using all the datapoints shown at $E(B-V) > 0.02 \text{ mag}$. The ratio $\Xi_{\text{HI}}/E(B-V)$ changes by only 45% over the range $0.02 \leq E(B-V) \leq 3 \text{ mag}$.

H I absorption (hence the presence of the cold neutral medium) is not consistently detected below $E(B-V) = 0.02 \text{ mag}$. This was noted by Kanekar et al. (2011) who described the lack of H I absorption for $N(\text{H I}) < 2 \times 10^{20} \text{ cm}^{-2}$. This implies a ratio $N(\text{H I})/E(B-V) = 10^{22} \text{ cm}^{-2} \text{ mag}^{-1}$

¹ For sightlines in common between the two datasets, the value from Liszt et al. (2010) has been retained

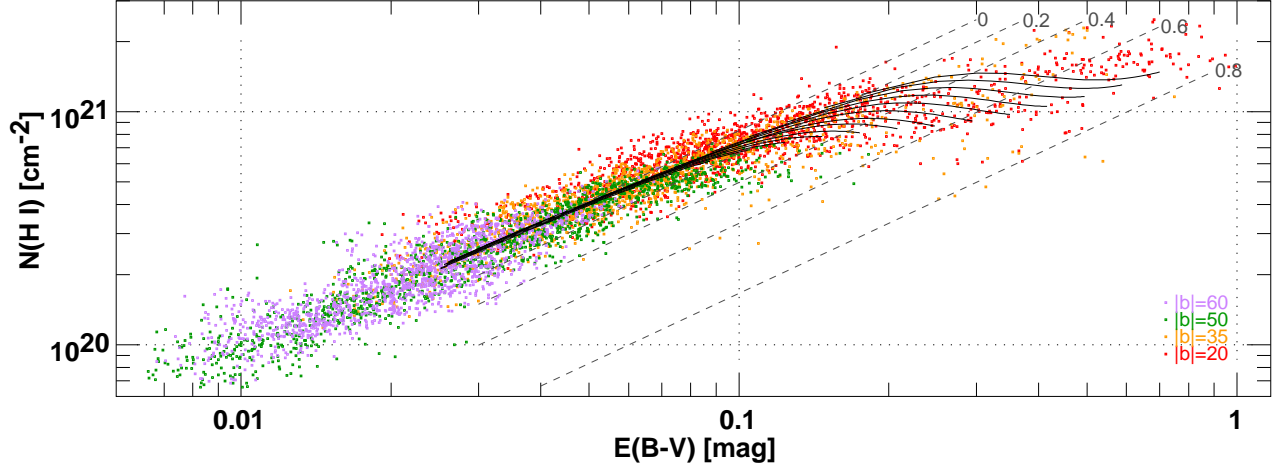


Fig. 1.— Reddening $E(B-V)$ from SFD98 and opacity-corrected LAB-survey H I column density $N(\text{H I})$. Data were sampled on grid points of the LAB survey at even 0.5° intervals around the sky at $b = \pm 20^\circ, \pm 35^\circ, \pm 50^\circ$ and $\pm 60^\circ$. Values of $N(\text{H I})$ were corrected as outlined in Sect. 2 and illustrated in Fig. 4. Dashed lines indicate loci of fixed molecular fraction $f_{\text{H}_2} = 1 - N(\text{H I})/N(\text{H})$ for $N(\text{H})/E(B-V) = 8.3 \times 10^{21} \text{ cm}^{-2} \text{ mag}^{-1}$. Solid lines correspond to models of H_2 -formation in low-density diffuse gas as discussed in Sect. 3.

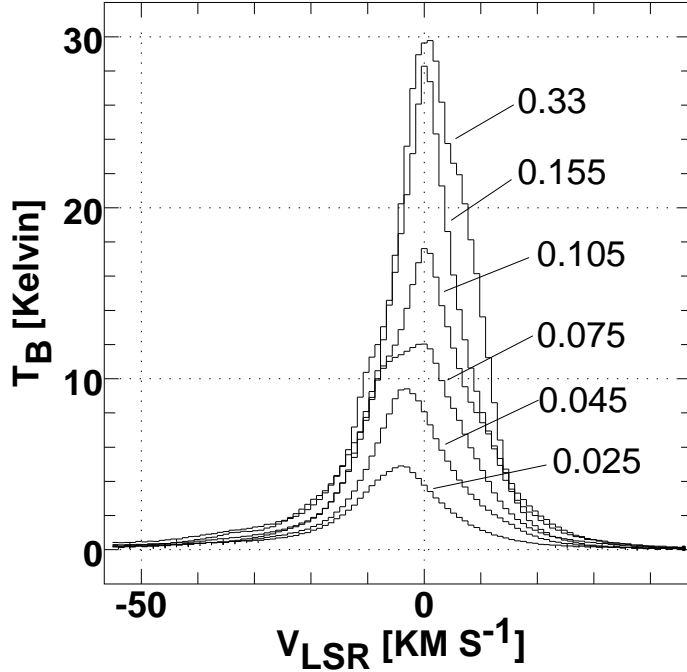


Fig. 2.— Mean H I profiles after binning the Fig. 1 data in $E(B-V)$ around $E(B-V)$ values $E(B-V) = 0.025, 0.045, \dots 0.33 \text{ mag}$ as indicated.

in keeping with the values found in our work but a more quantitative estimate can be derived from the table of Ξ_{HI} and optical-depth corrected $N(\text{H I})$ of Roy et al. (2013), from which it is found that $\langle N(\text{H I})/E(\text{B-V}) \rangle = 7.7 \pm 1.4 \times 10^{21} \text{ cm}^{-2} \text{ mag}^{-1}$.

Note that Fig. 3 appears to validate the use of $E(\text{B-V})$ from SFD98 up to rather higher values and at rather lower galactic latitudes than are usually believed to be reliable, see the discussion in the original work. Unlike the original discussion in Liszt et al. (2010) the relationship between Ξ_{HI} and $E(\text{B-V})$ is demonstrated over a wide range of galactic latitudes 1° - 60° .

2.2. Saturation correction to $N(\text{H I})$

A general saturation correction can be determined by constraining the derived column densities $N(\text{H I})$ to conform to the empirical Ξ_{HI} - $E(\text{B-V})$ relationship, where the free parameter connecting $N(\text{H I})$ to Ξ_{HI} is the spin temperature that is used to convert the observed brightness temperature profiles to $N(\text{H I})$. From the single power law for the Ξ_{HI} - $E(\text{B-V})$ relationship and the inflected variation of $N(\text{H I})$ with $E(\text{B-V})$ in Fig. 1 it may be inferred that there is a variation in the mean spin temperature with increasing $E(\text{B-V})$, actually a decline leading to a saturation correction that increases with $E(\text{B-V})$ as expected.

We began by deriving mean T_{sp} values from binned H I profiles (Fig. 2) across the range of $E(\text{B-V})$, assuming the power-law Ξ_{HI} - $E(\text{B-V})$ relationship shown in Fig. 3: these mean T_{sp} are shown in the upper panel of Fig. 4. Then we fit a smooth function to the variation of T_{sp} with $E(\text{B-V})$ and applied that to all H I profiles individually to correct them for the optical depth implied by their known reddening. This process is self-consistent in reproducing the power-law Ξ_{HI} - $E(\text{B-V})$ relationship when applied to the data at large. The power-law Ξ_{HI} - $E(\text{B-V})$ relation breaks down at $E(\text{B-V}) < 0.02 \text{ mag}$, $N(\text{H I}) < 2 \times 10^{20} \text{ cm}^{-2}$, leading to an underestimation of the mean T_{sp} , but no correction for saturation is needed at such small $N(\text{H I})$ anyway.

Fig. 4 at bottom shows the derived saturation correction as a multiplicative correction to the values of $N(\text{H I})$ derived from the mean H I profiles in the limit of zero optical depth, $N(\text{H I}) = 1.823 \times 10^{18} \text{ cm}^{-2} \int T_{\text{B}} d\nu$ with the integral expressed in units of K-km s^{-1} . Note that the T_{sp} variation and the corrections shown are relevant only to the data that was considered. A different dataset might require a different variation of T_{sp} with $E(\text{B-V})$ (see Section 4 below) and the magnitude of the correction that must be applied depends not only on T_{sp} but on the H I profile itself. When the profile integral is very small, even very small T_{sp} do not result in a significant correction to the optically thin value of $N(\text{H I})$. As well, the derived T_{sp} at a given $E(\text{B-V})$ might be very different for different datasets without implying significantly different correction factors at that $E(\text{B-V})$. The point is that $\Xi_{\text{HI}} \propto N(\text{H I})/T_{\text{sp}}$ by definition but $N(\text{H I})$ depends on T_{sp} only when

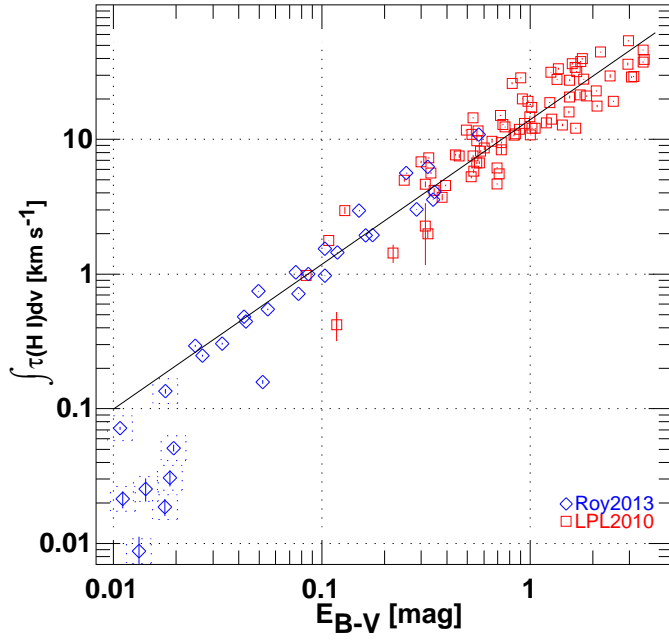


Fig. 3.— Velocity-integrated H I optical depth vs. reddening. The H I data are those of Liszt et al. (2010), taken from their work and from Dickey et al. (1983), and more recent results of Roy et al. (2013). The solid line is an error-weighted power-law fit to the data at $E(B-V) > 0.02$ mag, $\int \tau(HI)dv = 14.07 \text{ km s}^{-1} E(B-V)^{1.074}$. Errors in $E(B-V)$, not shown, are 16% according to SFD98.

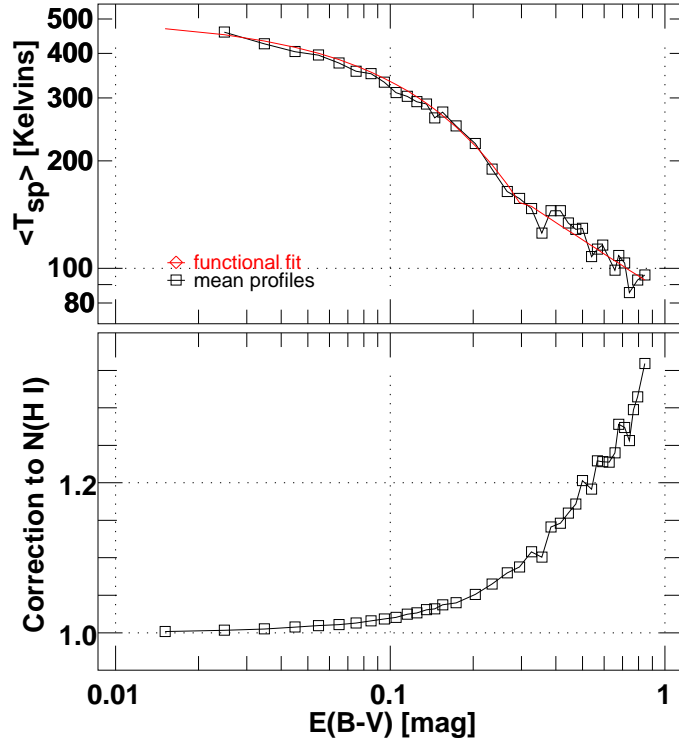


Fig. 4.— Top: mean spin temperature such that derived H I column densities conform to the power-law optical depth-reddening relationship shown in Fig. 3. The symbols represent the values for mean profiles binned in $E(B-V)$ (see Fig. 2) and the smooth curve is a fitted spin temperature function that was applied in Fig. 1. Bottom: The correction factor at each $E(B-V)$ that results from applying the spin temperature fit to the mean profiles binned in $E(B-V)$, expressed as a multiplicative factor for the infinitely optically thin H I column density.

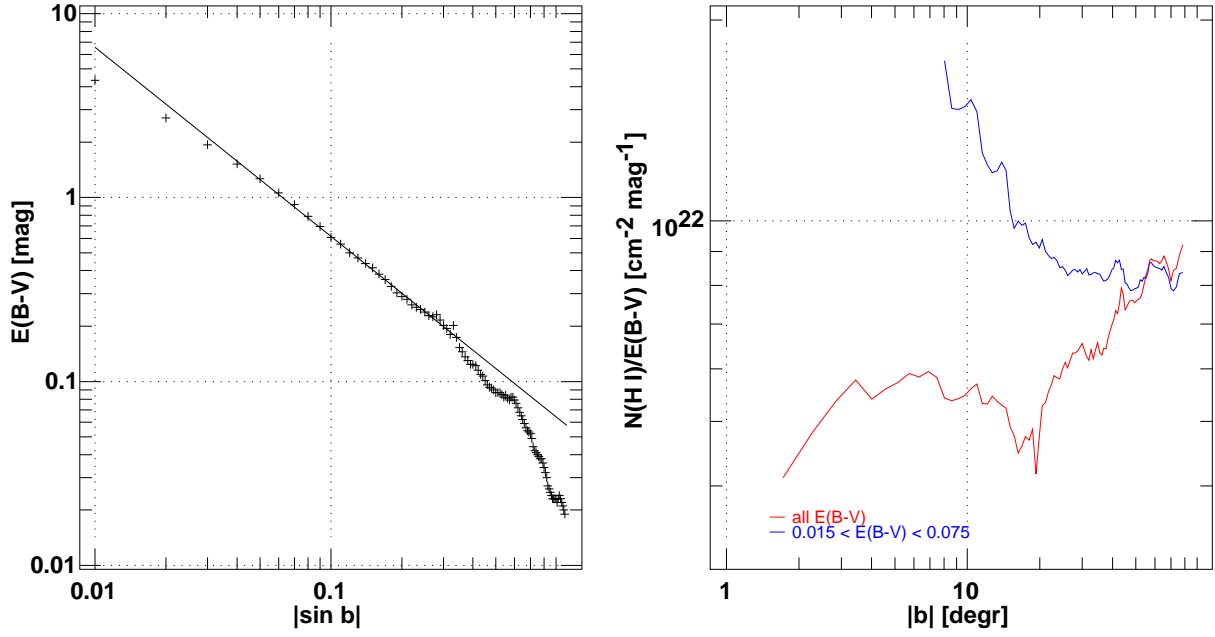


Fig. 5.— Left: mean $E(B-V)$ as a function of $\sin(|b|)$. Points were computed at steps of 0.01 in $\sin(|b|)$ at even 0.5° positions around the Galaxy as in Fig. 1. The solid line is a regression fit (power-law slope -1.028) to the points at $0.04 \leq \sin(|b|) \leq 0.3$. Right: $N(\text{H I})/E(B-V)$ averaged around the Galaxy at the latitudes used in the panel at left. Results are shown for all $E(B-V)$ (red, lower curve) and for $0.015 \leq E(B-V) \leq 0.075$ mag (blue, upper curve).

the optical depth is high.

In any case, the correction factor relevant to the dataset shown in Fig. 1 is below 20% for $E(B-V) < 0.5$ mag. In Liszt (2014) we used a constant $T_{\text{sp}} = 145$ K but the important ramifications of the data are the same. There is no appreciable correction to $N(\text{H I})$ at small $E(B-V)$, leading to a reliable value for $N(\text{H I})/E(B-V)$. The correction for saturation is not responsible for the inflection in the plot of $N(\text{H I})/E(B-V)$, which must be ascribed to the onset of H_2 -formation.

The relevance and accuracy of using a so-called isothermal correction to $N(\text{H I})$ given the optical depth absorption profile has recently been examined by Chengalur et al. (2013), who derive correction factors comparable to ours. The correction is described as isothermal because a single T_{sp} is applied at each velocity to emission that is a blend of contributions from different gas phases. The correction does an excellent job of bounding even very large errors in $N(\text{H I})$ that may occur at $\Xi_{\text{HI}} = 1\text{--}10 \text{ km s}^{-1}$ when the optical depth is unknown. The method adopted here is broader because we use an implied optical depth integral Ξ_{HI} to derive a single value of T_{sp} across an entire line profile but the conclusions are the same.

3. The influence of H_2 formation on $N(\text{H I})$

The empirical correction factors derived in Sect. 2 were applied to the data in Fig. 1 but a significant gap remains at $E(B-V) \gtrsim 0.1$ mag between the observed, corrected $N(\text{H I})$ and the straight line $N(\text{H I})/E(B-V) = 8.3 \times 10^{21} \text{ cm}^{-2} \text{ mag}^{-1}$ that is applicable below $E(B-V) = 0.08$ mag where H_2 -formation does not occur (Bohlin et al. 1978). That is also the line of zero molecular fraction, and superposed on the data are (dashed) lines of constant molecular hydrogen fraction $f_{\text{H}_2} = 1 - N(\text{H I})/N(\text{H})$, indicating very high molecular fractions at high $E(B-V)$.

Also shown in Fig. 1 are the results of a model calculation of H_2 -formation in a diffuse gas at low density $n(\text{H}) = 14 \text{ cm}^{-3}$. These are the same equilibrium heating/cooling/ H_2 -formation models we have used earlier in for instance Liszt (2007) to illustrate H_2 and CO formation, but now with the remainder H I shown on the vertical axis. Also, the models were calculated using the newly inferred value $N(\text{H})/E(B-V) = 8.3 \times 10^{21} \text{ cm}^{-2} \text{ mag}^{-1}$ that provides less dust shielding and extinction at a given $N(\text{H})$. Each leaf of the plot is for a separate cloud model having a central hydrogen column density $N(\text{H})$ differing by a factor $2^{1/4}$ from its neighbors and the variation along each leaf represents the locus of column density seen at all impact parameters across the face of the model. The right-most points along each leaf correspond to sightlines passing closer to the center of the model and so would be observed with smaller probability in real observations.

In any case, the point is to demonstrate that although there seems to be little alternative to H_2 -formation, that explanation also works in practice.

4. Latitude variation

Fig. 1 shows that the data at latitudes at $|b| \geq 20^\circ$ fit together into a coherent whole with a single message about $N(\text{H I})/E(\text{B-V})$ over the Galaxy and over a wide range of $E(\text{B-V})$. This is not true of the sky at smaller $|b|$, as will be discussed now.

Figure 5 at left shows the latitude variation of the mean reddening averaged around the sky. Below about 15° much of the sky is well-described by the cosecant law expected for a plane-parallel stratified medium. At higher latitudes the latitude dependence progressively steepens with, finally, a cubic dependence (actually, power-law -3.1) for $|b| > 36^\circ$. Given these gradients we worried that the larger H I beamsize of the LAB survey might have artificially increased the values we derived for $N(\text{H I})/E(\text{B-V})$. The disparity in beam sizes ($36'$ vs $6'$) would merely introduce scatter for a uniform sky, but the larger H I beam has a slightly lower intensity-weighted mean $|b|$ when viewing a medium that is concentrated to the galactic equator.

Numerical integration over the H I beam using the gradients shown in Fig. 5 suggested that the effect would not be important but as a test we recalculated our results comparing $N(\text{H I})$ with $E(\text{B-V})$ measured $9'$ and $18'$ closer to the galactic equator (ie 50% and 100% of the radius of the H I beam). We found only that the mean $N(\text{H I})/E(\text{B-V})$ declined progressively below $|b| = 8^\circ$, by a maximum of 5% at $|b| = 4^\circ$. The vertical sky gradient should not have affected any of the conclusions drawn in this work.

At the right in Figure 5 we show the variation in the mean $N(\text{H I})/E(\text{B-V})$ at $0.015 \leq E(\text{B-V}) \leq 0.075$ mag and over all $E(\text{B-V})^2$. $N(\text{H I})/E(\text{B-V})$ measured over the confined range varies little at $|b| \geq 20^\circ$, in keeping with Fig. 1, but increases rapidly down to $|b| = 8^\circ$, below which there are no LAB survey grid-points in the confined $E(\text{B-V})$ range. The mean $N(\text{H I})/E(\text{B-V})$ taken over all $E(\text{B-V})$ behaves oppositely, staying near $N(\text{H I})/E(\text{B-V}) = 5 - 6 \times 10^{21} \text{ cm}^{-2} \text{ mag}^{-1}$ at $|b| \lesssim 20^\circ$ and increasing above. The two curves increasingly coincide at larger $|b|$ where there are fewer positions with high reddening. The values $N(\text{H I})/E(\text{B-V}) = 5 - 6 \times 10^{21} \text{ cm}^{-2} \text{ mag}^{-1}$ measured over all $E(\text{B-V})$ at $|b| \lesssim 30^\circ$ may explain the difference between our results and those obtained previously (Savage et al. 1977; Shull & van Steenberg 1985; Diplas & Savage 1994) from stellar absorption spectra.

To better understand the latitude variation, Fig. 6 shows $N(\text{H I})/E(\text{B-V})$ for data at high and low $|b|$, binned in $E(\text{B-V})$. H_2 formation forces $N(\text{H I})$ down while the curves in Fig. 6 lay higher at smaller $|b|$ where the overall H_2 -fraction should be larger. Reconciling the low-latitude curves in Fig. 6 with a constant $N(\text{H I})/E(\text{B-V}) = 8.3 \times 10^{21} \text{ cm}^{-2} \text{ mag}^{-1}$ requires recognizing two effects:

² Note that we derived a separate saturation correction at $|b| < 20^\circ$ where profiles are broader, with smaller peak brightness and integrated opacity at a given $N(\text{H I})$ or $E(\text{B-V})$.

- i) The curves generally rise for smaller $|b|$ because sightlines at lower latitude and higher $E(B-V)$ are, somewhat counter-intuitively, less likely to be molecular. Only at low latitude is it possible to accumulate strong reddening over long pathlengths, in gas devoid of H_2 .
- ii) The low-latitude curves lie above the regression line. So either the gas/reddening ratio increases closer to the galactic plane or the curves must be shifted to the right. Very recent results from Planck Planck Collaboration et al. (2013) suggest just such a correction as noted in Section 5.

5. Discussion

When $E(B-V)$ from SFD98 is compared with 21cm H I column densities at $0.015 < E(B-V) < 0.075$ mag where H_2 -formation should be negligible, the stable ratio $N(H\ I)/E(B-V) = 8.3 \times 10^{21} \text{ cm}^{-2} \text{ mag}^{-1}$ derived at $|b| \geq 20^\circ$ substantially exceeds the seemingly universal value $N(H\ I)/E(B-V) = 4.8 - 5.2 \times 10^{21} \text{ cm}^{-2} \text{ mag}^{-1}$ that is derived from optical/uv absorption line work (Bohlin et al. 1978; Mirabel & Gergely 1979; Shull & van Steenberg 1985; Diplas & Savage 1994). Moreover the $N(H\ I)/E(B-V)$ ratio measured over the same restricted range of reddening increases strongly for $|b| \lesssim 20^\circ$, approximately doubling down to $|b| = 8^\circ$, at which point sightlines with $E(B-V) < 0.075$ mag do not exist in the data we considered at the gridpoints of the LAB all-sky H I survey,

At $|b| \gtrsim 20^\circ$, corrections to $N(H\ I)$ for optical depth in the 21cm line exceed 20% only at $E(B-V) \gtrsim 0.5$ mag, given the observed profiles and the integrated H I optical depth-reddening law we derived from interferometric H I absorption measurements, $\int \tau(HI) dv = 14.07 \text{ km s}^{-1} E(B-V)^{1.074}$ at $0.02 \lesssim E(B-V) \lesssim 3$ mag. Optical depth corrections to $N(H\ I)$ are even smaller at $10^\circ \lesssim |b| \lesssim 20^\circ$ where the galactic velocity gradient is more apparent and profiles have smaller peak 21cm brightness for a given $N(H\ I)$ and $E(B-V)$. In this case only H_2 -formation can be responsible for the inflection in the $N(H\ I)$ - $E(B-V)$ relationship that occurs at $E(B-V) \gtrsim 0.08$ mag and we showed model results for H_2 -formation in a low density diffuse gas that are a good match to the data.

In our earlier work we discussed possible corrections to the reddening maps of SFD98, based on previous work by other investigators; the prevailing view appeared to be that the reddening maps of SFD98, had, if anything, overestimated $E(B-V)$. Correcting the results of SFD98 in that manner would only exaggerate the effect discussed here. More recently the Planck dust maps have appeared (Planck Collaboration et al. 2013), and they may tell a different story. Although the Zodaical Emission-corrected 353 GHz optical depth maps converted to reddening give the same result we derived, $N(H\ I)/E(B-V) = 8.3 \times 10^{21} \text{ cm}^{-2} \text{ mag}^{-1}$, those maps are recommended for use only at larger $E(B-V)$. By contrast, the Planck reddening maps based on QSO colors that

are recommended for use below $E(B-V) = 0.3$ mag would have $E(B-V)' = (E(B-V)_{SFD} + 0.003 \text{ mag})/0.92$. When such a transformation is used to rederive the present results, we find a high-latitude asymptote $N(\text{H I})/E(B-V) = 7.2 \times 10^{21} \text{ cm}^{-2} \text{ mag}^{-1}$, accounting for about half the effect noted, in the log sense. This transformation increasing the $E(B-V)$ values of SFD98 at smaller $E(B-V)$ would shift the curves in Fig. 6 to the right in the manner required to reconcile them with a single value of $N(\text{H I})/E(B-V)$, as discussed in Sect. 4.

The National Radio Astronomy Observatory is a facility of the National Science Foundation operated under contract by Associated Universities, Inc. The author was partially funded by the grant ANR-09-BLAN-0231-01 from the French *Agence Nationale de la Recherche* as part of the SCHISM project (<http://schism.ens.fr/>). The author thanks Maryvonne Gerin for her hospitality at the ENS where this manuscript was finished. The author also thanks an anonymous referee for comments that served to clarify and improve the discussion.

REFERENCES

- Bohlin, R. C., Savage, B. D., & Drake, J. F. 1978, *ApJ*, 224, 132
- Chengalur, J. N., Kanekar, N., & Roy, N. 2013, *MNRAS*, 432, 3074
- Dickey, J. M., Kulkarni, S. R., Heiles, C. E., & Van Gorkom, J. H. 1983, *ApJS*, 53, 591
- Diplas, A. & Savage, B. D. 1994, *ApJ*, 427, 274
- Kalberla, P. M. W., Burton, W. B., Hartmann, D., et al. 2005, *A&A*, 440, 775
- Kanekar, N., Braun, R., & Roy, N. 2011, *ApJ*, 737, L33
- Liszt, H. 2014, *ApJ*, 780, 10
- Liszt, H. S. 2007, *A&A*, 476, 291
- Liszt, H. S., Pety, J., & Lucas, R. 2010, *A&A*, 518, A45
- Mirabel, I. F. & Gergely, T. E. 1979, *A&A*, 77, 110
- Peek, J. E. G., Heiles, C., Douglas, K. A., et al. 2011, *ApJS*, 194, 20
- Planck Collaboration, Abergel, A., Ade, P. A. R., et al. 2013, arXiv preprint, *astro-ph:1312.1300*, submitted to *A&A*

- Roy, N., Kanekar, N., Braun, R., & Chengalur, J. N. 2013, MNRAS, 436, 2352
- Savage, B. D., Drake, J. F., Budich, W., & Bohlin, R. C. 1977, ApJ, 216, 291
- Schlegel, D. J., Finkbeiner, D. P., & Davis, M. 1998, ApJ, 500, 525
- Shull, J. M. & van Steenberg, M. E. 1985, ApJ, 294, 599

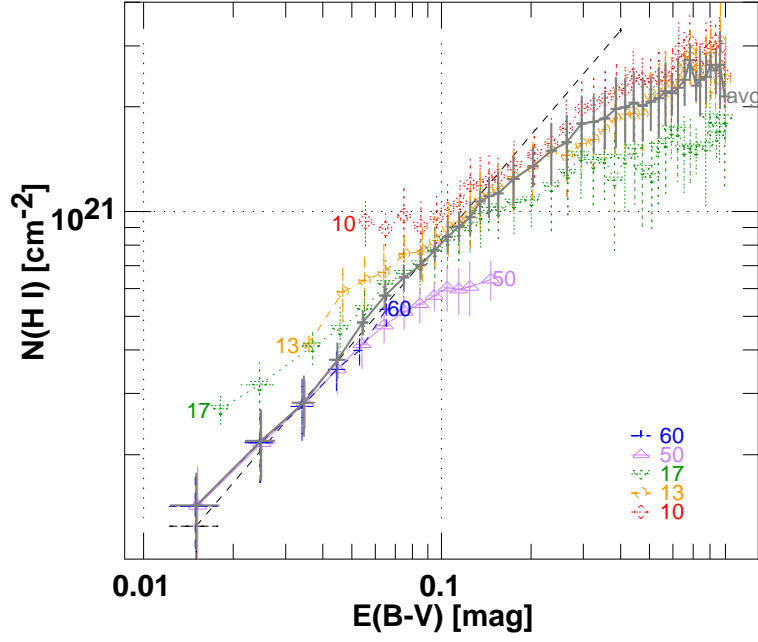


Fig. 6.— Like Fig. 1 but for binned data at high and low $|b|$. The mean of all data is shown as the solid black line. The dashed black line corresponds to $N(\text{H I})/E(\text{B-V}) = 8.3 \times 10^{21} \text{ cm}^{-2} \text{ mag}^{-1}$.